

# Tailored Aromatic Carbonyl Derivative Polyimides for High-Power and Long-Cycle Sodium-Organic Batteries

Heng-guo Wang, Shuang Yuan, De-long Ma, Xiao-lei Huang, Fan-lu Meng, and Xin-bo Zhang\*

Pressing concerns about limited reserve and distribution of lithium resources have led to an increasing interest in replacing lithium-ion batteries (LIBs) from a viewpoint of sustainability.<sup>[1–6]</sup> In response, sodium-ion batteries (NIBs) are an attractive alternative because sodium resources are practically inexhaustible and ubiquitous, for example, the cost of Na<sub>2</sub>CO<sub>3</sub> is only 3% of the cost of Li<sub>2</sub>CO<sub>3</sub>.<sup>[7–22]</sup> However, as only a very limited number of materials are reported to be viable up to now,<sup>[23,24]</sup> the performance of the NIBs is still terribly plagued by low specific capacity, poor rate capability, and short cycle life. On the other hand, the commonly used electrode materials in LIBs and NIBs are rely heavily on depletable metal-based inorganic compounds prepared from limited mineral resources, thus giving rise to the problem of cost and environmental concerns. Therefore, there is an urgent need to prepare future electrode materials, shifting from inorganic to organic materials that are more abundant, from renewable resources with minimum energy consumption. They are also required to have high power density and long cycling stability.

Organic materials, and in particular organic carbonyl compounds, are considered to be promising electrode materials due to their numerous advantages, including lightweight, redox stability, multi-electron reactions, and availability from easily accessible natural sources.<sup>[25–37]</sup> Furthermore, organic synthesis techniques and quantum chemical considerations enable the performance of batteries to be tuned on the molecular level, that is, to tailor secondary batteries.<sup>[25]</sup> Due to the less rigid structure compared to inorganic counterparts, organic compounds are structurally more flexible and thus could facilitate the higher mobility of large-sized sodium ions, which is vital to the operation of NIBs.<sup>[38]</sup> Furthermore, no strongly oxidizing substance would be generated during the charge/discharge process of organic materials, which could at least alleviate the daunting safety problem of the transition metal oxide (TMOs)

cathode.<sup>[29]</sup> In this context, very recently, organic carbonyl compounds, such as sodium terephthalate and its derivatives, have been developed as promising organic anodes for NIBs.<sup>[39–41]</sup> However, no corresponding organic compounds or aromatic carbonyl derivatives containing dianhydride as cathode materials for NIBs have been successfully developed until now because the direct implementation of organic molecules in battery systems is difficult due to the serious dissolution in electrolyte.<sup>[29,35,36]</sup> In response, one very promising strategy is to construct dianhydride-based polymer materials to make a stable and flexible framework, which could restrain the unwanted dissolution in the electrolyte and achieve fast kinetic properties.<sup>[29–32]</sup> Based on the structural characteristics of dianhydride, it is a promising alternative choice to construct dianhydride-based polyimides (PIs), which might also hold additional advantages such as good mechanical properties, high thermal stability, and low cost.

Here, a series of dianhydride-based PIs, which bear various commercially available dianhydrides such as pyromellitic dianhydride (PMDA), 1,4,5,8-naphthalenetetracarboxylic dianhydride (NTCDA), and perylene 3,4,9,10-tetracarboxylic dianhydride (PTCDA), are systematically proposed and synthesized by a facile one-pot reaction. Specifically, we first realize the synthesis of PTCDA-based PIs and demonstrate that all these PIs have excellent electrochemical performance as cathode materials for rechargeable NIBs due to their unique polymer structure composed of an alkyl chain interconnecting the electrochemically active centers. Among the polymers introduced, PTCDA-based PI has a high specific power of 20.99 kW kg<sup>-1</sup>, specific energy of 285 Wh kg<sup>-1</sup>, and over 5000 cycle life retaining 87.5% of its initial capacity in half-cells and thus show clear superiority over PMDA and NTCDA-based PI analogues because of its low solubility and the lowest unoccupied molecular orbital (LUMO) energy, which reveals a versatile yet unexplored strategy for the design of organic materials for NIBs.

Classically, PIs can be synthesized by a two-step polycondensation including solution polymerization and imidization from dianhydride and diamine.<sup>[42]</sup> Here, for the convenience of large-scale synthesis, a simple and straightforward one-pot solution polymerization route is used for the preparation of the polyimides. The synthesis route for dianhydride-based PIs is displayed in **Figure 1**. One of the key issues for a successful synthesis is the solubility of the respective dianhydride building block in solvent. Obviously, alteration of the aromatic system from PMDA to NTCDA or PTCDA lowers the solubility and thus fails to produce PTCDA-based PIs in common solvent. Here, quinoline is chosen as a suitable organic solvent to dissolve the starting materials and catalyze the polycondensation.

Dr. H.-g. Wang, S. Yuan, D.-l. Ma, X.-l. Huang,  
F.-l. Meng, Prof. X.-b. Zhang  
State Key Laboratory of Rare Earth Resource Utilization  
Changchun Institute of Applied Chemistry  
Chinese Academy of Sciences  
Changchun, 130022, P. R. China  
E-mail: xbzhang@ciac.ac.cn  
S. Yuan, D.-l. Ma, F.-l. Meng  
Key Laboratory of Automobile Materials  
Ministry of Education, and  
School of Materials Science and Engineering  
Jilin University  
Changchun, 130012, P. R. China



DOI: 10.1002/aenm.201301651

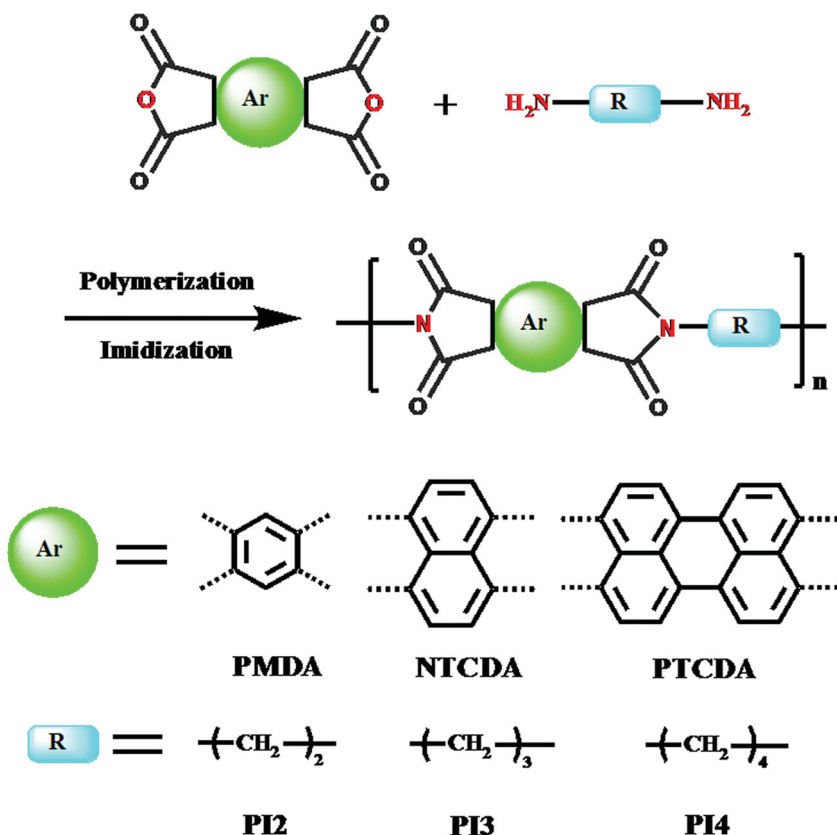


Figure 1. Synthesis route for various dianhydride-based PIs.

To demonstrate the feasibility of quinoline as an organic solvent for PTCDA, three aromatic PIs with different alkyl chain lengths from C2 to C4 to interconnect PTCDA are synthesized; these are named PI2, PI3, and PI4. The synthesis of these PIs is revealed by the Fourier transform infrared (FTIR) spectra (Supporting Information Figure S1a) and the characteristic FTIR bands are assigned in Supporting Information Table S1. The absence of the carbonyl (C=O) peaks for the amic acid and the presence of the C=O and C–N bonds for the imide confirm the completion of imidization and the successful polymerization of the three PIs. In addition, the consistency of their FTIR spectra indicates the similarity of their structures. Subsequently, the powder was slowly heated at 300 °C in vacuum oven for 2 h. By comparing the FTIR spectra before and after annealing (Supporting Information Figure S1b), it is observed that their structures are similar, which further demonstrates the completion of the imidization of the aromatic PIs prepared by a facile one-pot reaction. It is well-known that PIs are an engineering plastic with excellent thermally stability. To prove this point, the thermal properties of the PTCDA-based PIs are investigated by thermogravimetric analysis (TGA) and differential scanning calorimetry (DSC) techniques. As shown in Supporting Information Figure S2, all the three aromatic PIs show superior thermal stability compared to PTCDA, which is a very important property from the viewpoint of safety of NIBs.

Taking into account the benefit of chemical tunability of organic materials, we investigate the electrochemical performance of tailored aromatic carbonyl derivative polyimides. As

shown in Figure 2a,b, changing the conjugated backbone from PMDA to NTCDA and PTCDA increases the average discharge voltage from 1.73 to 1.89 and 1.94 V, which could be attributed to the difference of the lowest unoccupied molecular orbital (LUMO) energy resulting from the introduction of the additional electron-withdrawing groups.<sup>[30,35,36]</sup> For molecules closely related in structure, reduction potentials are linearly related to the LUMO energies.<sup>[43]</sup> Using density functional theory calculations, Andrzejak et al.<sup>[44]</sup> have demonstrated that altering the aromatic system from PMDA to NTCDA and PTCDA lowers the LUMO energy and thus the increased average discharge voltage from PMDA-based to NTCDA-based and PTCDA-based PIs is reasonable. We expect a substitution with much stronger electron-withdrawing groups, such as cyano and bromine, will enable further elevation of the redox potential of PIs. In addition, altering the conjugated backbone from PMDA to NTCDA and PTCDA reduces dissolution of PIs (Figure 2b, inset). For PMDA-based PIs, the capacity is rapidly reduced after the first cycle, and the retention is less than 50 mA g<sup>-1</sup> after 62 charge–discharge cycles. For NTCDA-based PIs, the capacity gradually decreases with cycling number, and moderate cycling stability is observed. However,

the situation for PTCDA-based PIs is much better: even after 150 charge–discharge cycles, 93.4 mA g<sup>-1</sup> is retained, indicating superior cycling stability, which is understandable in light of the low solubility of the PTCDA and choice of special organic solvent in the synthesis process. Furthermore, the decrease of alkyl chains can lead to reduced molecule weight, thus increasing the gravimetric capacity (Supporting Information Table S2). According to our observations, the gravimetric capacity of PI2 is much higher than those of PI3 and PI4 under the same experimental conditions (Figure 2c). Following the relationship, it is obvious that the structure of the dianhydride determines the working potentials, cycling stability, and gravimetric capacity. These results suggest that some of the operational characteristics of organic electrode materials could be predictably engineered with well-established synthesis strategies in organic chemistry, with the variation of conjugated backbone being an effective one.<sup>[36]</sup>

It is well known that the intrinsic electronic insulation of the organic materials results in unsatisfactory rate performance. Recently, the addition of large amounts of conductive carbon during electrode fabrication has been demonstrated as an efficient approach to improve the electron transport in electrodes, and thus highly utilizing the organic active materials.<sup>[28,32,35,36]</sup> Therefore, the change of PI2 loading is carried out (Supporting Information Figure S3). The decrease of PI2 loading from 80 wt% to 30 wt% results in a considerable capacity increment from 107.7 mAh g<sup>-1</sup> to 148.9 mAh g<sup>-1</sup> (Figure 3a). In order to clarify the capacity contribution, the charge–discharge curves of

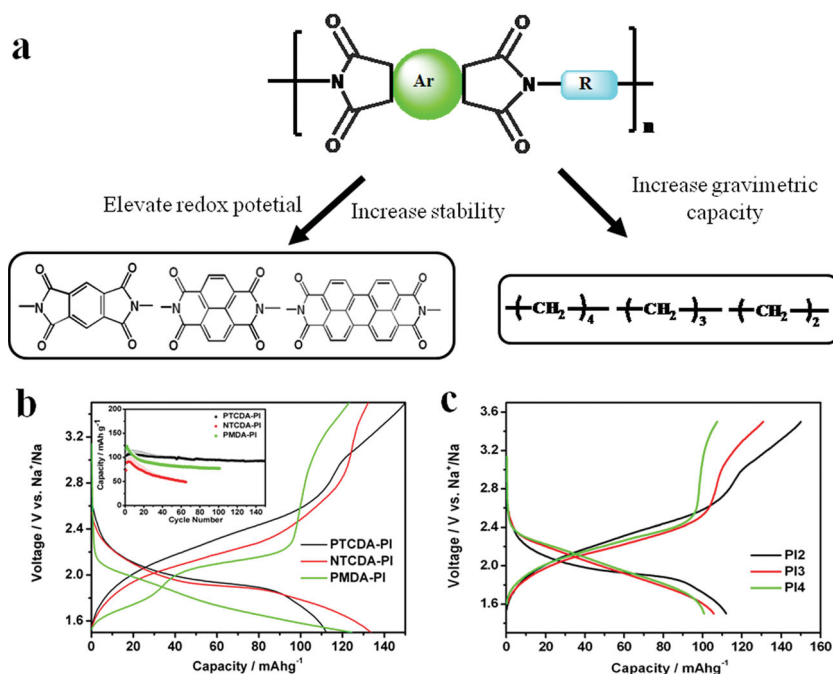


**Figure 2.** a) Chemical structures of tailored polyimides. b) Charge–discharge curves of different benzene-ring-based PIs electrodes at a current density of 25 mA g<sup>-1</sup> and cycle performance of different benzene ring-based PIs electrodes at a current density of 200 mA g<sup>-1</sup> (inset). c) Charge–discharge curves of different alkyl-chain-based PIs electrodes at a current density of 25 mA g<sup>-1</sup>.

carbon are measured and its specific capacity is only 14 mAh g<sup>-1</sup> (Supporting Information Figure S4). Therefore, most of the reversible capacity (about 134.9 mAh g<sup>-1</sup>) comes from the PI2, corresponding to a utilization ratio of 54.3% compared to the theoretical capacity (Supporting Information Table S2). That is to say, addition of conductive carbon could improve the carbonyl utilization.<sup>[28,37]</sup> Furthermore, it is noted that the charge–discharge curves deliver single voltage plateaus and no unwanted steps could be given in the voltage curves, which could appear for the Na<sup>+</sup>–Na<sup>+</sup> coulomb interactions in layered inorganic hosts for Na intercalation. The PI2 electrode retains a reversible capacity of 137.6 mAh g<sup>-1</sup> and a coulombic efficiency of 100% after 400 cycles, corresponding to a capacity retention ratio of 92.4% (Figure 3b). Unexpectedly, even at a high current density of 0.8 C, the PI2 electrode also delivers a reversible capacity of 110.8 mAh g<sup>-1</sup> even after 5000 cycles, corresponding to a capacity retention ratio of 87.5% (Figure 3c).

Additionally, the rate performance of the PI2 electrode is evaluated (Figure 3d). The reversible capacities are 137.1, 130.3, 127, 121.8, 112.7, 96.4, 75, and 50 mAh g<sup>-1</sup> at current densities of 0.2, 0.4, 0.8, 2, 4, 8, 20, and 40 C, respectively. Interestingly, even at a current density of 80 C, the PI2 electrode can also deliver 38.9 mAh g<sup>-1</sup>. Most importantly, when the current density is reduced after the back and forth high rate and 120 cycles measurement, a discharge capacity of 142.3 mAh g<sup>-1</sup>, which is comparable to the initial capacity in the first cycle, can be recovered. Then, the PI2 electrode retains a reversible capacity of 135.7 mAh g<sup>-1</sup> after 700 cycles at a current density of 0.1 C, demonstrating superior rate performance of the PI2 electrode. Figure 3d inset shows the PI2 electrode has an outstanding

high power of 20.99 kW kg<sup>-1</sup> and a high energy of 285 Wh kg<sup>-1</sup>. To the best of our knowledge, for organic electrode materials, the presented results indicate the best cycling stability, rate performance, and power density ever measured for LIBs, let alone NIBs.

The maximum amount of Na<sup>+</sup> ions that can be reversibly inserted/deinserted into the structure of PI2 is further determined by using the galvanostatic intermittent titration technology (GITT). By this means, the cell is operated under almost quasi-equilibrium conditions, which allows sufficient time for Na<sup>+</sup> ions to access the PI2 electrode, thus the obtained capacity can be seen as the theoretical capacity. To reduce the contribution from side reactions (mostly in the first cycle), we present the GITT charge/discharge curves of the second cycle (Figure 4a). It can be seen that the charge/discharge profile exhibits a similar curve shape and capacity to those the curves in Figure 3a, indicating that the obtained capacity is close to the theoretical capacity.

To unveil the mechanism of PI2 redox reaction with sodium, we have analyzed the change in the bonding nature of PI2 electrodes during battery operation using ex situ FTIR analysis (Figure 4b). For the as-prepared electrode, the absorbance signals at 1692.5 and 1662.4 cm<sup>-1</sup> can be attributed to the vibrational modes of the C=O double bonds in PI2. For the discharged electrode, peak shifting occurs, implying the formation of a new bond between oxygen and sodium. The peaks centered at about 1688 and 1651 cm<sup>-1</sup> can be attributed to the asymmetric and symmetric stretching vibration of the O–C–O–Na bond, which is similar to that of the O–C–O–Li bond.<sup>[45]</sup> The reversible recovery of the C=O double bonds in the recharged electrode coincides with the redox reaction of PI2 with sodium. Thus the reversible change in the C=O vibrational mode strongly supports the participation of C=O double bonds in the reversible reaction with sodium. However, the absorbance signals at 1588 and 1353 cm<sup>-1</sup> from the C=C stretching vibration of perylene and the C–N stretching vibration of imide, respectively, are unchanged, indicating that the perylene and imide in PI2 do not function as redox-active sites and participate in the reaction with sodium.

To understand in-depth how many sodium atoms can be inserted the aromatic dianhydride-based PI, further investigations were carried out. Theoretically, each formula unit of the prepared aromatic dianhydride-based PIs could experience the important enolization of the four carbonyl double bonds, which can be stabilized and promoted by conjugated structures. When the prepared PTCDA-based PIs are used as the cathode material in NIBs, each carbonyl group can receive one electron and be accompanied by the insertion of a sodium ion to form sodium enolate in the reduction process. The sodium ions are then deinserted in the reverse oxidation process. In the entire reduction and oxidation process, the perylene ring can keep the conjugated structure with the carbonyl groups

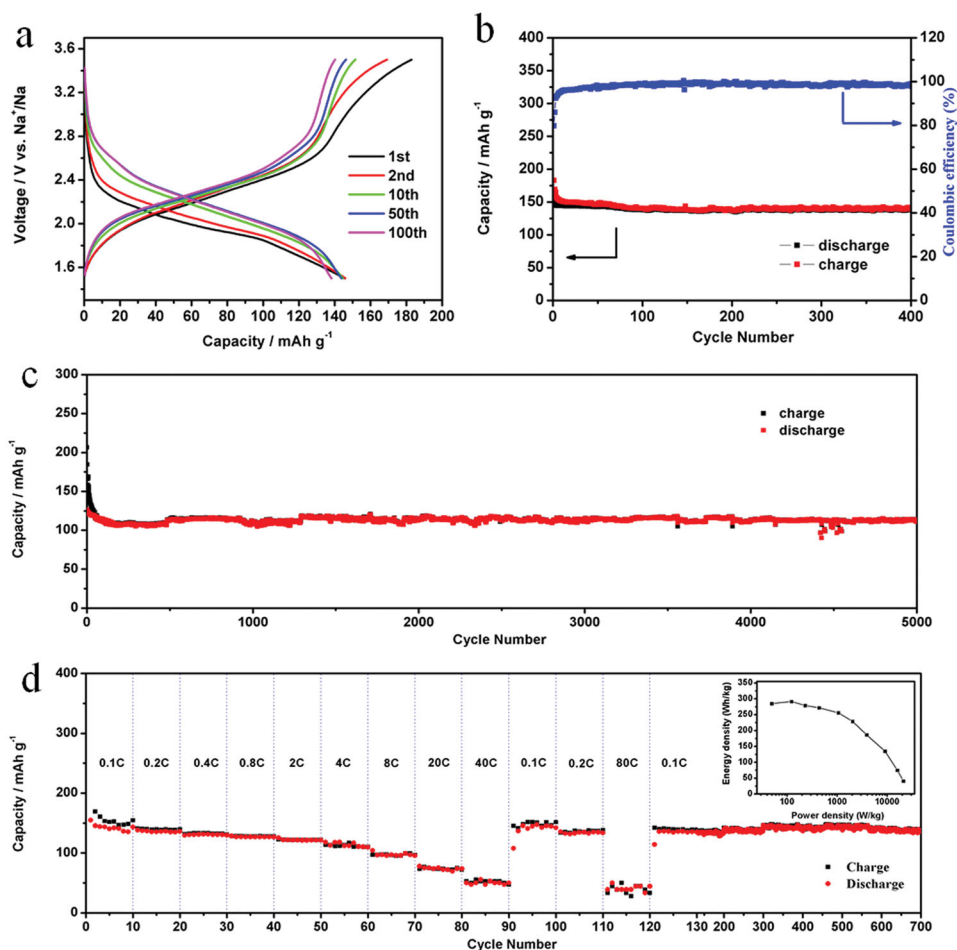


**Figure 3.** a) Charge–discharge curves and b) cycle performance of the PI2 electrode at a current density of 0.1 C. c) Cycle performance of the PI2 electrode at a current density of 0.8 C. d) Rate performance of the PI2 electrode at different current densities, inset: Ragone plots.

and promote the redox enolization reaction.<sup>[29]</sup> Ideally, each formula unit of the PIs transfers four electrons through two steps (Figure 4e), which may deliver a theoretical specific capacity of more than 240 mAh g<sup>-1</sup> (for PI2, Supporting Information Table S2). In the first-step discharge process, the PIs can capture two Na<sup>+</sup> ions at the opposite positions of carbonyl groups and then the perylene ring can form a conjugated structure with carbonyl groups and promote the redox enolization reaction. In the second-step discharge process, the other two opposite carbonyl groups can combine with two Na<sup>+</sup> ions to form sodium enolate. In practice, the second-step electrochemical reduction of the PIs for the last two-electron transfer can only be obtained under a deep-discharge below 1.5 V (Supporting Information Figure S5), which might be due to the repulsion between injected negative charges in the conjugated dianhydride unit.<sup>[29–31]</sup> Obviously, such a low-voltage deep-discharge process is not useful for PIs when proposed as a cathode material for NIBs. Thus, a potential range of 1.5–3.5 V is used to evaluate the electrochemical performance of the aromatic PI2 electrode. In the case of the reduction process, two carbonyl groups may generate a radical anion and then the dianion, and is accompanied by sodium ion association;

while in the case of the oxidation process, carbonyl groups are rebuilt and accompanied by sodium ion disassociation. However, the corresponding two pairs of well-resolved redox peaks can not be found in the cyclic voltammety (CV) curves of the PI2 electrode (Figure 4c), but the obviously broadened and split peaks are present. This result is similar to that reported by Song et al. and might be attributed to the fast transformation between the radical anion and dianion, and can possibly influence of the electrolyte.<sup>[30,31]</sup> In addition, the CV tests are conducted at various scan rates (Figure 4d) and the corresponding peak currents increase linearly with the scan rate, indicating that mass transfer might not be rate-determining for PI2 electrode.<sup>[32]</sup>

The above-obtained superior electrochemical performance, including high specific capacity, long cycle life, and good rate performance, is attributed to the incorporation of the conductive carbon and the specific characteristics of this unique PI polymer framework. The electronic conductivity of PI2 is significantly enhanced by incorporating large amounts of conductive carbon during electrode fabrication. Higher conductive carbon loading can further increase the carbonyl utilization and the electronic conductivity, thus improving the rate

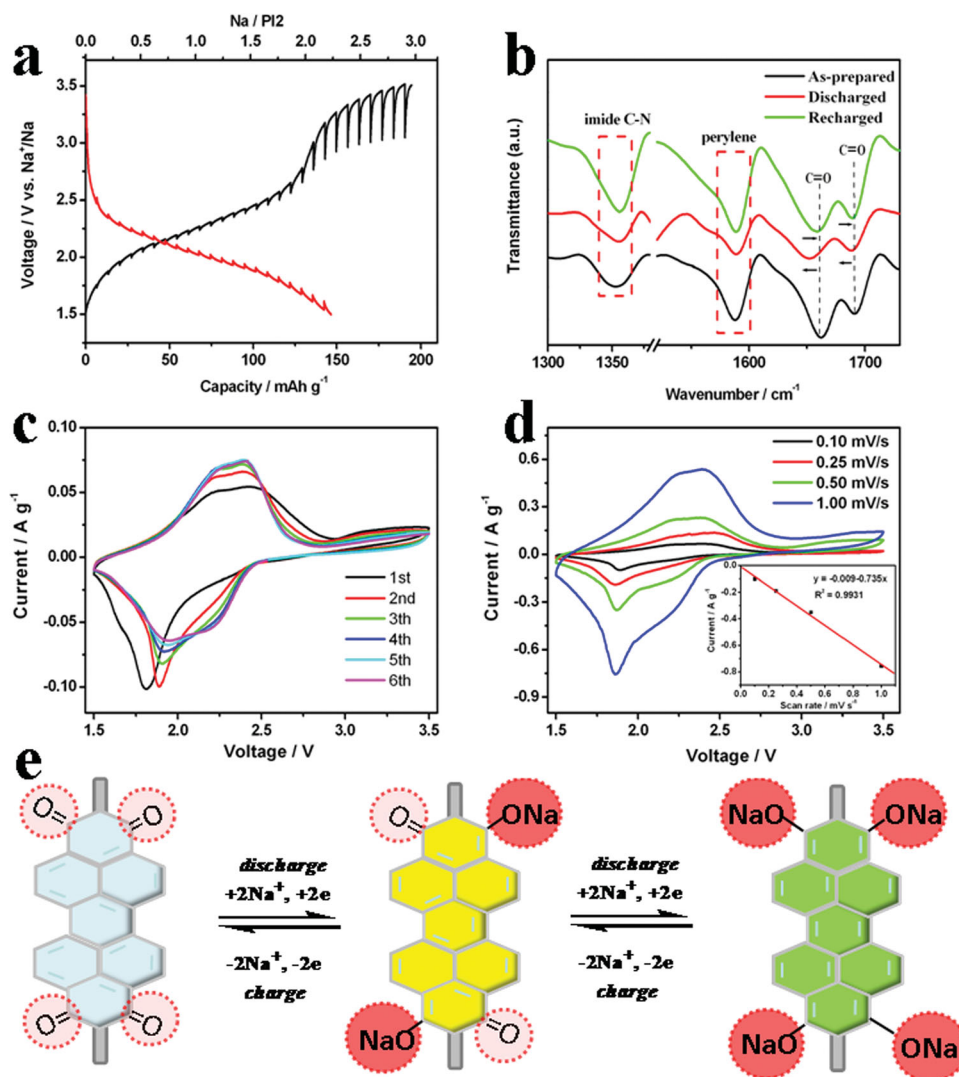


**Figure 4.** a) The second cycle of the charge/discharge curves using GITT mode: on each current step, the cell was charge or discharged at 0.1 C for 15 min; between two current steps, an interrupt time of 15 min was used to relax the cell to a quasi-equilibrium state. b) FTIR spectra of the PI2 electrode at different states of charge. CV curves of the PI2 electrode between 1.5 and 3.5 V c) at a scan rate of 0.1 mV s<sup>-1</sup> and d) at various scan rates from 0.1 to 1.0 mV s<sup>-1</sup>. Inset: the relationship between the peak current density and the scan rate. e) Schematic diagram for the proposed reversible electrochemical redox mechanism of PTCDA-based PIs.

performance. However, the superior electrochemical performance is not simply a result of the introduction of higher conductive carbon loading. Instead, it mainly originates from the unique polymer structure composed of the well alkyl chain interconnecting the electrochemically active center PTCDA to form the polymer framework structure, which greatly inhibits the unwanted dissolution in the electrolyte and thus improves the stability. To fully demonstrate the superiority of the polymer structure, different electrochemical measurements are carried out as follows. First, successive measurements are carried out with the loading of active materials (PI2) set at a high value (60%). As shown in Supporting Information Figure S6, the PI2 electrode also shows excellent electrochemical performances including a carbonyl utilization ratio of 45%, specific capacity (112 mAh g<sup>-1</sup>), long cycle life (5800 cycles), and good rate performance. Thus, the low loading of the active

materials during electrode fabrication also results in more satisfactory battery performance. Second, the electrochemical performance of PTCDA-based PIs with different alkyl chain lengths ranging from C2 to C4 is also investigated (Supporting Information Figure S7). All the three PIs electrodes exhibit superior cycle life even when the current rate increases from 25 to 200 mA g<sup>-1</sup>. They also show similar charge–discharge mechanism that PTCDA is the active centers for sodium ion insertion–deinsertion in the polymer framework, which consolidates the promise of PTCDA-based PIs as electrode materials in NIBs. Finally, we compare the PI2 electrode for lithium insertion and sodium insertion to prove the superiority of the organic materials used as NIBs. As shown in Supporting Information Figure S8a and Figure S6a, the sodium insertion voltage is found to be lower than the lithium insertion voltage, which could be attributed to the less positive redox potential

of sodium ( $-2.71$  V vs SHE (standard hydrogen electrode)) compared to lithium ( $-3.02$  V vs SHE). Fortunately, the reduction voltage could be increased by using established strategies in organic electrochemistry, for example, incorporating the electron-withdrawing group.<sup>[35,36]</sup> In addition, as shown in Supporting Information Figure S8b and Figure S6b, the electrochemical performance of the sodium insertion is comparable to that of the lithium insertion, indicating that organic materials could provide higher mobility of large-sized sodium ions because of their structural flexibility, which can effectively improve the poor kinetics of the sodium ion de/insertion reaction caused by its larger ionic radius compared to the lithium cation. Therefore, organic materials are an attractive choice to make NIBs replace LIBs.

In summary, we have developed high-performance organic sodium batteries materials using tailored aromatic carbonyl-derivative polyimides. PTCDA-based PIs deliver a high specific power of  $20.99$  kW kg<sup>-1</sup> and specific energy of  $285$  Wh kg<sup>-1</sup>, and over 5000 cycle life retaining 87.5% of its initial capacity. Furthermore, the use of PTCDA improves the working potentials and cycling stability compared with those of PMDA and NTCDA-based PIs. Besides the attractive electrochemical performance of the proposed materials, our findings suggest that the advantage of the organic materials is tailored molecular design for battery engineering. We anticipate that the successful material design for organic cathode materials described here will lead to improved strategies and will greatly broaden the scope for future investigations of next generation NIBs.

## Experimental Section

**Synthesis of PTCDA-Based PIs:** Equimolar PTCDA and diamine (ethylene diamine, 1,3-propanediamine, or 1,4-diaminobutane) were added in quinoline at room temperature. After stirring for 6 h, the mixture was heated at reflux under nitrogen for 12 h, cooled to room temperature, and poured into 1 M NaOH solution. Then the suspended reaction mixture was filtrated, washed repeatedly with water, NaOH solution (1 M), and acetone, and dried under vacuum at  $150$  °C for 12 h.

**Characterization:** The morphology of as-obtained samples was characterized using scanning electron microscopy (SEM, Hitachi S-4800). Thermogravimetric analysis was performed on a NETZSCH STA 449 F3 simultaneous TGA-DSC instrument from 0 to  $800$  °C in N<sub>2</sub> with a heating rate of  $10$  °C min<sup>-1</sup>. FTIR measurements were performed on a Bruker IFS 66V/S spectrometer using KBr pellets.

**Electrochemical Measurements:** The electrodes were prepared by mixing active material (60 wt%), acetylene black (30 wt%), and polyvinylidene fluoride (PVDF, 10 wt%) in *N*-methyl-2-pyrrolidone (NMP). For the optimization of the electrochemical performance of the PI2, the electrode composition was changed to active material (30 wt%), acetylene black (60 wt%), and PVDF (10 wt%). After the slurries were uniformly spread onto an aluminum foil, the electrodes were dried at  $80$  °C in vacuum for 8 h. The electrodes were then pressed and cut into disks before transferring into an argon-filled glove box. Coin cells (CR2025) were assembled in the laboratory using sodium metal as the counter electrode, Celgard 2400 membrane as the separator, and NaPF<sub>6</sub> (1 M) in ethylene carbonate/dimethyl carbonate (EC/DMC, 1:1 w/w) as the electrolyte. Galvanostatic charge-discharge tests were carried out on a Land Battery Measurement System (Land, PR China). The cells were galvanostatically discharged and charged at various C rates (here 1C refers to  $250$  mAh g<sup>-1</sup> for PI2). CV was performed using a VMP3 Electrochemical Workstation (Bio-logic Inc.).

## Supporting Information

Supporting Information is available from the Wiley Online Library or from the author.

## Acknowledgements

This work was financially supported by the 100 Talents Programme of the Chinese Academy of Sciences, National Natural Science Foundation of China (Grant No. 21101147 and 21203176), China Postdoctoral Science Foundation (2011M500624), and Special Foundation of China Postdoctoral Science (2012T50293).

Received: October 30, 2013

Revised: November 11, 2013

Published online: December 5, 2013

- [1] J.-M. Tarascon, *Nat. Chem.* **2010**, *2*, 510.
- [2] S. Xin, L. Gu, N.-H. Zhao, Y.-X. Yin, L.-J. Zhou, Y.-G. Guo, L.-J. Wan, *J. Am. Chem. Soc.* **2012**, *134*, 18510.
- [3] C. F. Zhang, H. B. Wu, C. Z. Yuan, Z. P. Guo, X. W. Lou, *Angew. Chem. Int. Ed.* **2012**, *51*, 9592.
- [4] Z. W. Seh, W. Y. Li, J. J. Cha, G. Y. Zheng, Y. Yang, M. T. McDowell, P.-C. Hsu, Y. Cui, *Nat. Commun.* **2013**, *4*, 1331.
- [5] L. Qie, W.-M. Chen, Z.-H. Wang, Q.-G. Shao, X. Li, L.-X. Yuan, X.-L. Hu, W.-X. Zhang, Y.-H. Huang, *Adv. Mater.* **2012**, *24*, 2047.
- [6] G. L. Cui, L. Gu, L. J. Zhi, N. Kaskhedikar, P. A. van Aken, K. Müllen, J. Maier, *Adv. Mater.* **2008**, *20*, 3079.
- [7] N. Yabuuchi, M. Kajiyama, J. Iwatate, H. Nishikawa, S. Hitomi, R. Okuyama, R. Usui, Y. Yamada, S. Komaba, *Nat. Mater.* **2012**, *11*, 512.
- [8] J. F. Qian, M. Zhou, Y. L. Cao, X. P. Ai, H. X. Yang, *Adv. Energy Mater.* **2012**, *2*, 410.
- [9] Y. L. Cao, L. F. Xiao, W. Wang, D. Choi, Z. M. Nie, J. G. Yu, L. V. Saraf, Z. G. Yang, J. Liu, *Adv. Mater.* **2011**, *23*, 3155.
- [10] Z. L. Jian, W. Z. Han, X. Lu, H. X. Yang, Y.-S. Hu, J. Zhou, Z. B. Zhou, J. Q. Li, W. Chen, D. F. Chen, L. Q. Chen, *Adv. Energy Mater.* **2013**, *3*, 156.
- [11] Y. Sun, L. Zhao, H. Pan, X. Lu, L. Gu, Y.-S. Hu, H. Li, M. Armand, Y. Ikuhara, L. Chen, X. Huang, *Nat. Commun.* **2013**, *4*, 1870.
- [12] Z. L. Jian, L. Zhao, H. L. Pan, Y.-S. Hu, H. Li, W. Chen, L. Q. Chen, *Electrochem. Commun.* **2012**, *14*, 86.
- [13] L. Wang, Y. H. Lu, J. Liu, M. W. Xu, J. G. Cheng, D. W. Zhang, J. B. Goodenough, *Angew. Chem. Int. Ed.* **2013**, *52*, 1964.
- [14] K. Tang, L. J. Fu, R. J. White, L. H. Yu, M.-M. Titirici, M. Antonietti, J. Maier, *Adv. Energy Mater.* **2012**, *2*, 873.
- [15] A. Darwiche, C. Marino, M. T. Sougrati, B. Fraisse, L. Stievano, L. Monconduit, *J. Am. Chem. Soc.* **2012**, *134*, 20805.
- [16] H.-G. Wang, Z. Wu, F.-L. Meng, D.-L. Ma, X.-L. Huang, L.-M. Wang, X.-B. Zhang, *ChemSusChem* **2013**, *6*, 56.
- [17] K. Saravanan, C. W. Mason, A. Rudola, K. H. Wong, P. Balaya, *Adv. Energy Mater.* **2013**, *3*, 444.
- [18] H. Kim, R. A. Shaker, C. Park, S. Y. Lim, J. S. Kim, Y. N. Jo, W. Cho, K. Miyasaka, R. Kahrman, Y. Jung, J. W. Choi, *Adv. Funct. Mater.* **2013**, *23*, 1147.
- [19] V. Palomares, P. Serras, I. Villaluenga, K. B. Hueso, J. Carretero-González, T. Rojo, *Energy Environ. Sci.* **2012**, *5*, 5884.
- [20] S. Komaba, W. Murata, T. Ishikawa, N. Yabuuchi, T. Ozeki, T. Nakayama, A. Ogata, K. Gotoh, K. Fujiwara, *Adv. Funct. Mater.* **2011**, *21*, 3859.
- [21] B. L. Ellis, L. F. Nazar, *Curr. Opin. Solid State Mater. Sci.* **2012**, *16*, 168.

- [22] S. Wenzel, T. Hara, J. Janek, P. Adelhelm, *Energy Environ. Sci.* **2011**, 4, 3342.
- [23] H. L. Pan, Y.-S. Hu, L. Q. Chen, *Energy Environ. Sci.* **2013**, 6, 2338.
- [24] S.-W. Kim, D.-H. Seo, X. H. Ma, G. Ceder, K. Kang, *Adv. Energy Mater.* **2012**, 2, 710.
- [25] Y. Morita, S. Nishida, T. Murata, M. Moriguchi, A. Ueda, M. Satoh, K. Arifuku, K. Sato, T. Takui, *Nat. Mater.* **2011**, 10, 947.
- [26] M. Armand, S. Grugeon, H. Vezin, S. Laruelle, P. Ribière, P. Poizot, J.-M. Tarascon, *Nat. Mater.* **2009**, 8, 120.
- [27] H. Y. Chen, M. Armand, G. Demailly, F. Dolhem, P. Poizot, J.-M. Tarascon, *ChemSusChem* **2008**, 1, 348.
- [28] W. Guo, Y.-X. Yin, S. Xin, Y. G. Guo, L.-J. Wan, *Energy Environ. Sci.* **2012**, 5, 5221.
- [29] X. Han, C. Chang, L. Yuan, T. Sun, J. Sun, *Adv. Mater.* **2007**, 19, 1616.
- [30] Z. Song, H. Zhan, Y. Zhou, *Angew. Chem. Int. Ed.* **2010**, 49, 8444.
- [31] Z. Song, H. Zhan, Y. Zhou, *Chem. Commun.* **2009**, 448.
- [32] T. Nokami, T. Matsuo, Y. Inatomi, N. Hojo, T. Tsukagoshi, H. Yoshizawa, A. Shimizu, H. Kuramoto, K. Komae, H. Tsuyama, J.-i. Yoshida, *J. Am. Chem. Soc.* **2012**, 134, 19694.
- [33] K. Sakaushi, G. Nickerl, F. M. Wisser, D. Nishio-Hamane, E. Hosono, H. S. Zhou, S. Kaskel, J. Eckert, *Angew. Chem. Int. Ed.* **2012**, 51, 7850.
- [34] K. Sakaushi, E. Hosono, G. Nickerl, T. Gemming, H. S. Zhou, S. Kaskel, J. Eckert, *Nat. Commun.* **2013**, 4, 1485.
- [35] Y. Liang, P. Zhang, J. Chen, *Chem. Sci.* **2013**, 4, 1330.
- [36] Y. Liang, P. Zhang, S. Yang, Z. Tao, J. Chen, *Adv. Energy Mater.* **2013**, 3, 600.
- [37] Z. P. Song, T. Xu, M. L. Gordin, Y.-B. Jiang, I.-T. Bae, Q. F. Xiao, H. Zhan, J. Liu, D. H. Wang, *Nano Lett.* **2012**, 12, 2205.
- [38] A. L. Goodwin, *Nat. Mater.* **2010**, 9, 7.
- [39] L. Zhao, J. M. Zhao, Y.-S. Hu, H. Li, Z. B. Zhou, M. Armand, L. Q. Chen, *Adv. Energy Mater.* **2012**, 2, 962.
- [40] Y. Park, D. S. Shin, S. H. Woo, N. S. Choi, K. H. Shin, S. M. Oh, K. T. Lee, S. Y. Hong, *Adv. Mater.* **2012**, 24, 3562.
- [41] A. Abouimrane, W. Weng, H. Eltayeb, Y. J. Cui, J. Niklas, O. Poluektov, K. Amine, *Energy Environ. Sci.* **2012**, 5, 9632.
- [42] M. K. Ghosh, K. L. Mittal, *Polyimides: Fundamentals and Applications*, Marcel Dekker, New York **1996**.
- [43] A. Kuhn, K. G. von Eschwege, J. Conradie, *J. Phys. Org. Chem.* **2012**, 25, 58.
- [44] M. Andrzejak, G. Mazur, P. Petelenz, *J. Mol. Struct.* **2000**, 527, 91.
- [45] X. Y. Han, G. Y. Qing, J. T. Sun, T. L. Sun, *Angew. Chem. Int. Ed.* **2012**, 21, 5147.